Available online at www.sciencedirect.com
SCIENCE DIRECT
Journal of Catalysis 236 (2005) 335–345
JOURNAL OF CATALYSIS
www.elsevier.com/locate/jcat

On the paradox of transition metal-free alumina-catalyzed epoxidation with aqueous hydrogen peroxide

Roberto Rinaldi, Ulf Schuchardt *

Instituto de Química, Universidade Estadual de Campinas, PO Box 6154, 13083-970 Campinas-SP, Brazil

Received 29 June 2005; revised 3 October 2005; accepted 7 October 2005

Available online 10 November 2005

Abstract

The aluminas obtained by calcination of nanocrystalline boehmite, prepared by the sol–gel method, in the range 200–1000 °C were characterized by powder X-ray diffraction, thermogravimetric analysis, Fourier transformed infrared spectroscopy, nitrogen adsorption–desorption, and scanning electron microscopy. The catalytic activity of these aluminas in the epoxidation of *cis*-cyclooctene with aqueous 70 wt% hydrogen peroxide shows, after 24 h, a profile with two maxima at 400 and 700 °C that corresponds to 85 and 80% yield, respectively. However, this profile cannot be directly related to the structural and textural properties of the calcined aluminas. Regarding the hydrophilicities of the calcined aluminas, determined by the amount of water molecules per nm^2, the epoxide yield of the aluminas can be segregated into three groups corresponding to the general crystallographic classification of these aluminas: boehmite, γ-series, and δ-series. The aluminas from the γ-series show the highest cyclooctene oxide yield after 1 h; however, due to surface modifications occurring during the reaction, the aluminas from the δ-series also give good yields after 24 h. The water adsorption capacity or hydrophilicity of these aluminas shows a strong correlation with epoxide productivity of the calcined aluminas at 24 h. Generally, better epoxide productivity is observed for lower hydrophilicities. The hydrogen peroxide efficiencies are typically 2.0–2.5 mmol of oxidant per mmol of epoxide formed after 24 h. However, the aluminas of the δ-series show poor efficiency at the beginning of the reaction that improves from an average of 4.1 to 2.3 mmol of oxidant per mmol of epoxide after 2 h due to modification of their surfaces.

Keywords: Sol–gel alumina; Textural properties; Chemical properties; Surface hydrophilicity; Catalytic epoxidation; Hydrogen peroxide

1. Introduction

Aluminum oxides or aluminas are a group of inorganic chemicals currently produced in very large volumes [1]. An increasing amount of alumina is being applied in the chemical industry for fillers, adsorbents, catalysts, ceramics, abrasives, and refractories, although production of aluminum metal consumes ca. 90% of all alumina [1,2]. In heterogeneous catalysis, alumina is used in many industrial catalytic processes as both a catalyst and a support for catalytically active components [1,2]. In several instances, the alumina support contributes to the catalytic activity and so assumes an essential role in the catalytic system [3]. The "term alumina" encompasses ionic solids with formula $Al_2O_3{\cdot}(H_2O)_n$, where n is 0–3, although none actually contains water [4]. The calcination of crystalline or amorphous aluminum hydroxides or oxyhydroxides in the 200–1200 °C range results in several transition aluminas with structures depending on the precursor, final temperature, and mode of heating [2,5,6]. Thermal treatment causes a formal loss of water through desorption of physically bound water or condensation of vicinal hydroxyl groups [2,4,7] and leaves behind an exposed Al^{3+} ion, which, because of its electron deficiency, behaves as a Lewis acid site. However, some hydroxyl groups remain on the surface during the thermal treatment of aluminum hydroxide or oxyhydroxides, which may act as proton donors (Brønsted acid sites) [8]. Of all types of defects created during dehydration, the triplet vacancies are assumed to have the greatest catalytic importance in the solid–gas interface. They provide unusual exposure of the aluminum ions in the underlying layer and constitute strong Lewis acid sites [11–13]. Furthermore, not only does the surface undergo a progressive change during the thermal treating of aluminum hydroxides or oxy-hydroxides, but also the structure is significantly transformed during heating

* Corresponding author. Fax: +55 19 37883023.
E-mail address: ulf@iqm.unicamp.br (U. Schuchardt).

0021-9517/$ – see front matter
doi:10.1016/j.jcat.2005.10.007

in the range 200–1200 °C. Heating up to 600 °C, for example, yields the γ-series of alumina containing ρ, χ, η, and γ-Al_2O_3 with $Al_2O_3{\cdot}(H_2O)_n$, where $n < 0.6$ [2,4]. The thermal treatment carried out in the range ca. 800–1200 °C produces the δ-series of alumina containing very few hydroxyl groups on the surface ($n \sim 0$) and including the κ, θ, and δ varieties, which are more crystalline than the aluminas from the γ-series [2,4]. The endpoint in the phase transition occurs by heating the materials above 1200 °C to produce corundum, one of the hardest substances known and the most thermodynamically stable form of Al_2O_3 [4,9].

When exposed to water or moisture, the surfaces of the transition aluminas become hydrated, yielding a surface layer of hydroxyl groups [10–12]. This rehydration may change the structure of transition aluminas, but does result in deactivation of the higher-energy sites, such as the triplet vacancies. Knözinger's model is the most complete approach for understanding the hydroxyl surface groups of γ-Al_2O_3 [8]; however, this model is only a good approach for the gas–solid interface. In a water-containing reaction system, greater complexity of alumina surface groups is expected, taking into consideration the interaction with water molecules. A recent review describes the chemistry of alumina in the aqueous interface [13].

Aluminas are used by organic chemists as catalysts or as supports for reagents or catalysts to obtain fine chemicals [14,15]. In a joint project with Roger A. Sheldon's group, we showed that only alumina effectively heterogenizes homogeneous rhenium epoxidation catalysts [16]. However, under epoxidation conditions, alumina itself was already active for the epoxidation of cyclooctene and cyclohexene with anhydrous hydrogen peroxide in ethyl acetate under catalytic conditions [16]. The epoxidation activity of alumina had been reported previously [17], but the reactions showed low epoxide yields using a large excess of alumina and oxidant. Our subsequent investigation [18] showed that alumina catalytic systems were also useful for the epoxidation of terpenes and 1-olefins when using anhydrous hydrogen peroxide with selectivities usually in the 70–90% range. We were able to achieve productivities of up to 4.3 g epoxides per g of alumina [18]. In a parallel paper [19] we reported that the yields of epoxides were normally >70% and that very few byproducts were formed. Investigations of the alumina system have clearly shown that the reaction occurs at the surface [19,24]. To our surprise, various commercial chromatographic aluminas (acidic, neutral, and basic) showed similar catalytic behavior for the epoxidation of α-pinene using anhydrous hydrogen peroxide [19]. However, ultrapure aluminas prepared using four different sol–gel routes showed different yields of (*S*)-limonene and cyclohexene epoxides [20]. Using sol–gel alumina, we showed that anhydrous hydrogen peroxide solutions can be replaced by aqueous 70 wt% hydrogen peroxide with improvements in catalyst lifetime, allowing the catalyst to be recycled for four times and obtaining an overall yield of ca. 56 g of cyclooctene oxide per g of alumina [22]. The reactivity observed for the different substrates—namely that electron rich alkenes have the highest reactivity—is consistent with a "normal" electrophilic mechanism [19,21]. Apparently the weakly or moderate acidic sites, Al–OH, are exchanged during the reaction by hydroperoxo groups, forming activated Al–OOH species, which epoxidize nucleophilic alkenes [19,22,23]. In a recent study [24], we discovered that surface hydrophilicity plays a pivotal role in the catalytic activity of γ-Al_2O_3 and that the key factor responsible for the similar catalytic behavior of commercial chromatographic aluminas is a similar hydrophilicity. In contrast, γ-Al_2O_3 obtained from thermal heating of boehmites synthesized by sol–gel methods showed different hydrophilicities related to their different catalytic behaviors [20,24]. Standard techniques of acidity and basicity characterization, such as TPD-NH_3 and TPD-CO_2, do not suffice for understanding the catalytic activity of our system, because the acidic and basic surface properties determined by these experiments are valid only for a "cleaned" surface obtained during pretreatment [24]. But the alumina surface under reaction conditions is completely rehydrated, as either aqueous hydrogen peroxide is used or water is produced during the reaction. Thus the Lewis acid sites, –O–Al^+–O–, are transformed into Brønsted acid sites, Al–OH or Al–OH_2^+. Under reaction conditions, the acid strength of these sites is weak to moderate, as strong acid sites are expected to react with the epoxide to form a considerable amount of ring-opened byproducts [24,25].

In this paper we show how the hydration of the alumina surface is the key factor for the understanding of the relationship between structural, textural, and chemical properties of aluminas, calcined in the range 200–1000 °C, and their catalytic activity and hydrogen peroxide efficiency.

2. Experimental

2.1. Synthesis of the catalysts

The precursor of the calcined aluminas, boehmite, was obtained by the hydrolysis of aluminum *sec*-butoxide (Merck, 99.8%). In a 500-mL three-necked round-bottomed flask, 72.00 g of ultrapure water (Milli-Q) were added, under mechanical stirring, to 240.00 g of 50 wt% aluminum *sec*-butoxide in *sec*-butanol (Merck, p.a.). (Caution: This reaction is highly exothermic.) The mixture obtained was stirred for 5 min, at which point it was transformed into a homogeneous gelatinous slurry. This gel was placed in a rectangular glass plate (17 × 28 cm) and dried at 120 °C for 24 h, producing the xerogel. About 3.0–4.0 g of xerogel were calcined under a static atmosphere at 200, 300, 400, 500, 600, 700, 800, and 1000 °C giving the material herein denominated A-200, A-300, A-400, A-500, A-600, A-700, A-800, and A-1000. The xerogel was heated at 1 °C/min until each temperature level was reached, where it was maintained for 3 h. At the final heating step, the temperature was maintained for 24 h. For mild rehydration, the calcined aluminas A-200 to A-1000 were left in an oven at 100 °C for 24 h. The materials were then stored in closed flasks in a desiccator over silica gel and molecular sieves of 3 Å for subsequent characterization and epoxidation reactions.

2.2. Catalyst characterization

2.2.1. X-Ray power diffraction

Powder X-ray diffraction (XRD) patterns were determined with a Shimadzu XD-3A diffractometer, using Cu-K_α radiation and 2θ from 5° to 90°, with a step size of 0.02° and counting time of 3 s. The apparent crystallite size of the xerogel was determined using Scherrer's equation along the (020) reflection of the boehmite. Corundum with a crystallite size of 1 μm was used as internal standard.

2.2.2. Fourier transformed infrared spectroscopy

The Fourier transform infrared (FTIR) spectra were recorded using 64 scans of 400–1600 cm^{-1} in a Bomen infrared spectrometer (MB series; Hartmann and Braun) with a resolution of 4 cm^{-1}. Analysis was performed by grinding samples together with KBr (1 wt%).

2.2.3. Surface area analysis

The nitrogen adsorption–desorption isotherms of calcined aluminas were measured on a Micrometrics ASAP 2010 device. The samples were degassed at 120 °C under vacuum (1 μbar) for 3 h. The surface area was determined by adsorption–desorption of nitrogen at 77 K. The pore volume and average pore diameter were calculated using the BET method.

2.2.4. Scanning electron microscopy

Secondary electron images were acquired in a JEOL JSM 6360 LV scanning electron microscope, operating at 20 kV. The samples were placed on brass stubs and coated with carbon followed by a gold and palladium (80 and 20%) coating in a Bal-Tec MD 020 instrument (20 s, 30 μA). To determine particle diameter distribution, 256 particles were manually measured for each image.

2.2.5. Thermogravimetric analysis

Thermogravimetric analysis (TGA) of the calcined aluminas were carried out under an oxidative atmosphere (synthetic air, 100 mL/min) using a TA Micrometrics 2950 TGA instrument with a heating rate of 20 °C/min in the range 30–900 °C. The analyses were performed in duplicate for each sample.

2.2.6. Elemental analysis

Elemental analyses were carried out using a Perkin–Elmer Series II CHN S/O Analyzer model 2400. Calcined alumina samples were mixed with an oxidant mixture (Pb_3O_4/NaF, 1:7), and the elemental analysis was performed by combusting the samples at 925 °C. The analyses were done in triplicate.

2.3. Catalytic reactions

The aqueous solution of hydrogen peroxide (70 wt%) was supplied by Peróxidos do Brasil S.A. (Solvay) and used without further treatment. The reaction solution was prepared to contain 1.00 mol/L of *cis*-cyclooctene (Acros; 95%) and 0.500 mol/L of *n*-butylether (internal standard; Acros; >99%) in ethyl acetate (Merck; p.a.).

In a two-necked round-bottomed flask, 20.00 mL of the reaction solution (20.0 mmol of cyclooctene and 10.0 mmol of *n*-butylether) were placed, and 2.00 mL (56 mmol) of aqueous 70 wt% H_2O_2 solution was added. The mass of the reaction mixture was determined for calculation of the hydrogen peroxide content. This mixture was heated to 80 °C with magnetic stirring. An initial aliquot ($t = 0$ h) was taken for gas chromatography (GC) analysis, and the reaction was started by adding the alumina (200.0 mg). Aliquots (50 μL) were taken at 1, 2, 4, 8, 12, and 24 h; diluted in hexane (2 mL; Tedia, high-performance liquid chromatography); and treated with a few milligrams of manganese dioxide to promote decomposition of the peroxides and then with anhydrous sodium sulfate to remove residual water. These solutions were analyzed using a Hewlett–Packard HP 5890 Series II gas chromatograph equipped with an Alltech AT-WAX capillary column (20 m × 0.25 mm × 0.25 μm film thickness) and a flame ionization detector. The *cis*-cyclooctene epoxide was quantified using a calibration curve obtained with a standard solution. Selectivity is always given with respect to converted *cis*-cyclooctene.

2.4. Determination of hydrogen peroxide

In an Erlenmeyer flask, 50 mL of an aqueous 20 wt% acetic acid solution and 20 g of dry ice for deaeration of the solution were added. After 2 min, ca. 2.0 g of potassium iodide (Synth; p.a.) and 3 drops of a 1 wt% ammonium molybdate solution (Vetec; p.a.) were added. To this mixture, 200-mg aliquots of the reaction mixture, collected at 0, 1, 2, 4, 8, 12, and 24 h, were added. The iodine formed was titrated with a 0.1000 mol/L solution of sodium thiosulfate (Synth; p.a.). Near the endpoint of the titration (pale brown color), 1.0 mL of a 1-wt% starch solution was added. The endpoint was detected when the blue color disappeared. The amount of H_2O_2, in mmol, in the reaction mixture was calculated by

$$n_{H_2O_2} = \frac{C_{S_2O_3^{2-}} \cdot V_{S_2O_3^{2-}}}{2} \cdot \frac{m_{\text{reaction}}}{m_{\text{aliquot}}} \times 10^3, \quad (1)$$

where $C_{S_2O_3^{2-}}$ is the concentration of the sodium thiosulfate solution (mol/L), $V_{S_2O_3^{2-}}$ is the volume of sodium thiosulfate solution (L), m_{reaction} is the reaction mixture mass (g), and m_{aliquot} is the mass of the aliquot (g) taken after 0, 1, 2, 4, 8, 12, and 24 h. To determine the H_2O_2 content at 1, 2, 4, 8, 12, and 24 h, the alumina mass was considered as the mass of the reaction mixture.

3. Results and discussion

Elemental analysis of the xerogel indicated that the carbon content was negligible, about 0.2 wt%, within the experimental error of our equipment. In previous reports [22,24] we used oxalic acid as a gelation catalyst to obtain nanocrystalline boehmite. But this resulted in a higher carbon content in the xerogel (5.8 wt%) and in the alumina calcined at 400 °C (0.8 wt%). In the present study we replaced the gelation catalyst (oxalic acid) by rapid hydrolysis with no aging of the gel, to obtain a nanocrystalline boehmite precursor with much lower

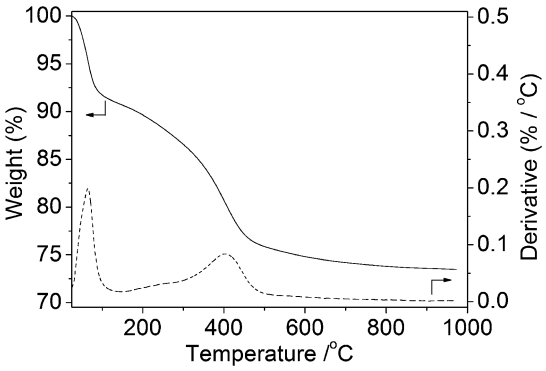

Fig. 1. TG curve of the xerogel.

Table 1
Crystalline phase assignment for the calcined aluminas

Identification	$T_{calcination}$ (°C)	Phase present
Xerogel	–	Boehmite
A-200	200	Boehmite
A-300	300	Boehmite
A-400	400	Boehmite + γ-Al_2O_3
A-500	500	γ-Al_2O_3
A-600	600	γ-Al_2O_3
A-700	700	δ-Al_2O_3
A-800	800	δ-Al_2O_3 + θ-Al_2O_3
A-1000	1000	θ-Al_2O_3

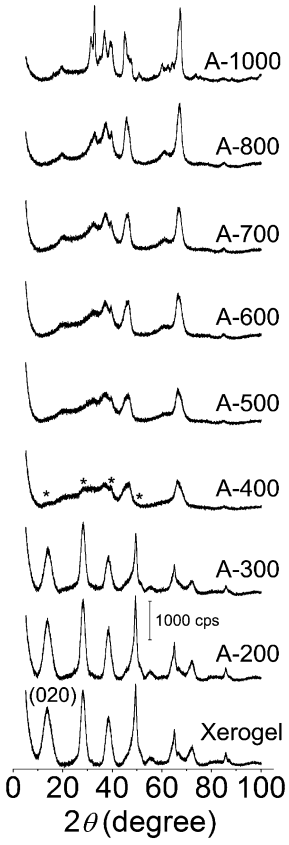

Fig. 2. XRD patterns of the xerogel and the aluminas calcined at 200 to 1000 °C. The asterisks at the A-400 XRD pattern indicate the presence of boehmite phase.

carbon content. The lower carbon content is important for accurately determining the water molecules per nm^2 of alumina surface (vide infra).

The thermogravimetric curve of the xerogel synthesized is shown in Fig. 1. The weight losses are due mainly to dehydration and dehydroxylation of the material. As the figure shows, the xerogel contains ca. 25 wt% of water in its structure and/or on its surface. The TGA curve shows four regions of weight loss: (i) room temperature–ca. 110 °C, due to desorption of physically bonded water; (ii) ca. 110–290 °C, corresponding to desorption of water chemically bonded onto the boehmite; (iii) ca. 300–500 °C, corresponding to dehydroxylation during the phase transition of boehmite to γ-Al_2O_3; and (iv) above 500 °C, due to dehydration of γ-Al_2O_3 and posterior phase transitions ($\gamma \rightarrow \delta \rightarrow \theta$-$Al_2O_3$) [26,27].

Fig. 2 shows the thermal evolution of the xerogel structure in the range 200–1000 °C by XRD patterns. Table 1 gives the phase attributions for the calcined aluminas.

The boehmite-to-γ-Al_2O_3 phase transition represents a total reorganization of the atoms in the lattice. Boehmite can be a well-ordered solid; its structure composed of double chains of AlOOH forming double layers arrayed in a cubic stacking sequence [2,28]. The aluminum ions are only in octahedral positions. However, this structure is totally lost when γ-Al_2O_3 is obtained. The aluminum atoms in γ-Al_2O_3 are partly in tetrahedral and partly in octahedral positions, forming a so-called "defect" spinel structure, in which the oxygen atoms are in the cubic closely packed layers [2,28]. In the normal $M^{3+}M^{2+}$ (AB_2O_4) spinel, 32 oxygen anions and 24 cations compose the unit cell. However, only $21\frac{1}{3}$ Al^{3+} ions are available for cation positions, resulting in cation vacancies in the case of γ-Al_2O_3 [29]. The oxygen sublattice is fairly well ordered, although there is significant disorder in the tetrahedral aluminum sublattice [30]. There are many open questions regarding the formation, structure, and even stoichiometry of γ-Al_2O_3 [2,30]. In the range 400–600 °C a consolidation of the γ-Al_2O_3 structure occurs. At 700 °C, the structure of the alumina is more organized than those observed for A-400 and A-500, resulting in a pattern characteristic of δ-Al_2O_3. Indeed, only small differences between the γ-Al_2O_3 and δ-Al_2O_3 structures are observed in the XRD patterns. For A-800, it is also possible to observe the presence of θ-Al_2O_3, which is more crystalline than γ-Al_2O_3 or δ-Al_2O_3. The transition of γ- to θ-Al_2O_3 through δ-Al_2O_3 does not require a reconstructive recrystallization process, because of the similar cubic, closely packed oxygen sublattice [5,31]. The ordering of structure increases due to the alignment and merging of lamellae and stacking faults in the (111) direction and from diffusion of the surface aluminum ions to more ordered sites [5,32]. At 1000 °C, the material is more crystalline, and only θ-Al_2O_3 is observed (Fig. 2).

In some cases it is not easy to identify the mixture of different alumina phases, because of their broad XRD patterns. However, Priya et al. [33] showed that FTIR spectra in the range 1600–400 cm^{-1} may be a useful tool for monitoring the phase transitions for highly crystalline boehmite samples. The boehmite structure contains only octahedral aluminum atoms

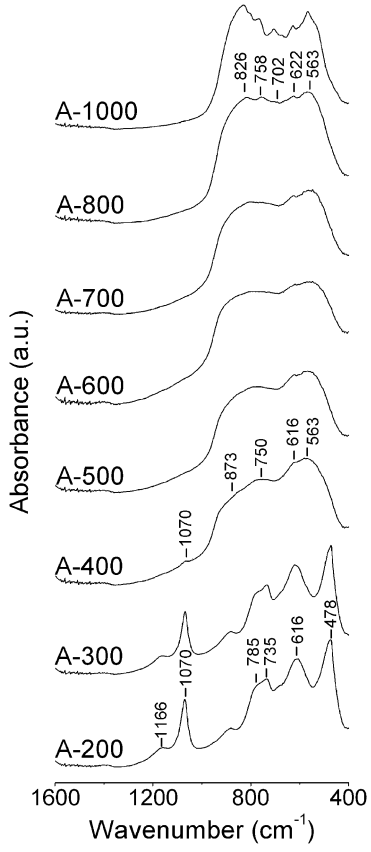

Fig. 3. FTIR spectra for the aluminas calcined at 200–1000 °C.

and has Al–OH groups on the lamellae surfaces, and thus is expected to show the stretching and perhaps also the bending modes of octahedral aluminum (AlO_6), which fall around 500–750 cm^{-1} and 350–450 cm^{-1}, respectively [33]. The bending mode of Al–O–H in the boehmites is expected to be around 900–1100 cm^{-1} [34]. The transition aluminas contain both tetrahedral and octahedral aluminum ions. The stretching and bending modes of tetrahedral aluminum (AlO_4) appear in the narrow ranges of 750–850 cm^{-1} and 250–320 cm^{-1}, respectively [33]. Stretching and bending modes of octahedral aluminum (AlO_6) in transition aluminas are believed to occur in the same regions described for boehmite [33].

Fig. 3 shows the FTIR spectra of aluminas calcined at 200–1000 °C. For the boehmites A-200 and A-300, the band at 478 cm^{-1} is assigned to the bending mode of (AlO_6) units, and the bands at 616 and 735 cm^{-1} are assigned to (AlO_6) stretching modes. The intense band at 1070 cm^{-1} and a shoulder at 1166 cm^{-1} are due to symmetric and asymmetric bending modes of Al–O–H groups, respectively. The shoulder at 785 cm^{-1} is assigned to the OH torsional mode [33]. As mentioned above, the phase transition of boehmite to γ-Al_2O_3 represents a total rearrangement of the lattice, forming new octahedral and tetrahedral aluminum sites. It can be clearly seen that the 400–900 cm^{-1} region is completely different for A-400, which is mainly γ-Al_2O_3. The presence of boehmite in A-400 can be more easily detected by the presence of the band at 1070 cm^{-1} in the FTIR spectrum (Fig. 3) than by the XRD pattern of A-400 (Fig. 2). The shoulder at 873 cm^{-1} is assigned to the (AlO)$_4$ stretching mode. In contrast to more crystalline alumina [33], the overlapping of the different stretching and bending modes of (AlO_6) and (AlO_4) units is quite strong for nanocrystalline transition aluminas, not allowing differentiation of the bands related to each vibrational mode of the tetrahedral and octahedral Al–O units. In our study, however, even with this strong overlap between the bands, it is possible to observe that the structure of alumina A-800 is somewhat different from that of A-700, because some peaks appear in the 400–800 cm^{-1} region. Although the XRD patterns for A-700 and A-800 are quite similar, the FTIR spectrum suggests that A-800 is probably a mixture of both δ-Al_2O_3 and θ-Al_2O_3 (Fig. 3). The A-1000 alumina is clearly assigned as θ-Al_2O_3 by the XRD pattern (Fig. 2), and its FTIR spectrum shows some similarities with the A-800 alumina spectrum, clearly confirming the coexistence of both δ-Al_2O_3 and θ-Al_2O_3 in A-800.

Table 2
Textural properties of the calcined aluminas

Alumina	Surface area (m^2/g)	Pore volume (cm^3/g)	Average pore diameter (nm)
A-200	380	1.93	20.2
A-300	363	1.90	20.8
A-400	370	2.11	22.4
A-500	325	2.08	25.7
A-600	295	2.08	28.1
A-700	253	1.98	31.3
A-800	173	1.31	30.5
A-1000	139	1.18	33.2

The evolution of the textural properties of the aluminas was determined by nitrogen adsorption–desorption isotherms at 77 K (Fig. 4). Table 2 summarizes the textural properties for aluminas A-200 to A-1000.

All of the aluminas calcined in the range 200–1000 °C show a type II isotherm with H_3 hysteresis (Fig. 4). This indicates that the porosity of the material is nonstructural and is due to intraparticular voids. Typically, this type of hysteresis is found in slit-shaped pores between the particles, which are sufficiently large that capillary condensation occurs only at a relative pressure close to $P/P_0 = 1$ [35]. The alumina particles are strongly bonded to on another by hydrogen bonds between Al–OH groups. With increasing calcination temperature, these Al–OH groups are extensively removed, and the packing of the particles becomes weaker, resulting in an apparent increase of the average pore diameter. This is not the only effect of increasing calcination temperature; sintering of the small particles can also occur. This sintering is the main reason for the progressive decrease in surface area for alumina calcined above 500 °C.

Scanning electron micrographs for the calcined aluminas show that the particles of all calcined aluminas are composed of clusters of spheres (Fig. 5) resulting in a cauliflower-like morphology. Nevertheless, it is possible to see that the sizes of these spheres and their aggregates changed at different calcination temperatures. The morphology for the particles is the same for all aluminas studied. The void spaces between these clusters make slits that form the nonstructural mesopores in the synthesized materials. These mesopores are of the same order of mag-

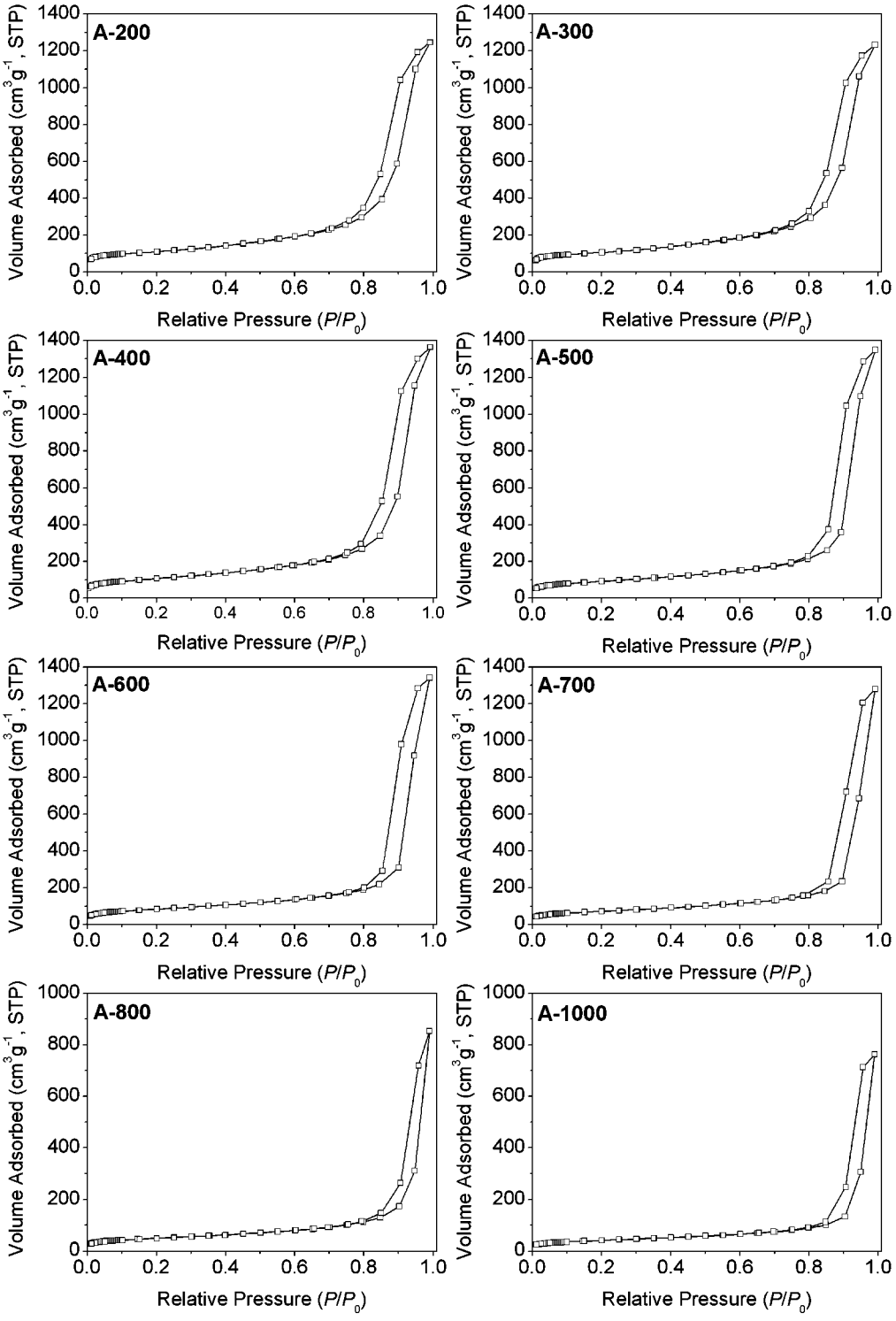

Fig. 4. Nitrogen adsorption–desorption isotherms at 77 K of aluminas A-200 to A-1000.

nitude as those determined by nitrogen adsorption–desorption isotherms (Table 2).

The heating of alumina at different temperatures causes increased dispersivity of particle diameters (Fig. 6) and also of average particle diameter (Table 3). This results from sintering of the particles, which consumes smaller particles and creates medium-sized and larger particles, increasing the dispersivity of the particle diameters.

The surface of the calcined aluminas is rehydrated when exposed to water (from atmospheric air or from the reaction mixture). The extent of this process depends on the structural and textural properties [11,12]. TGA of the aluminas as used in the catalytic reactions (calcined in at 200–1000 °C and mildly rehydrated at 100 °C for 24 h) was done to evaluate the total amount of water (physically and chemically bonded) on the alumina surfaces. The weight losses can be assigned mainly to the

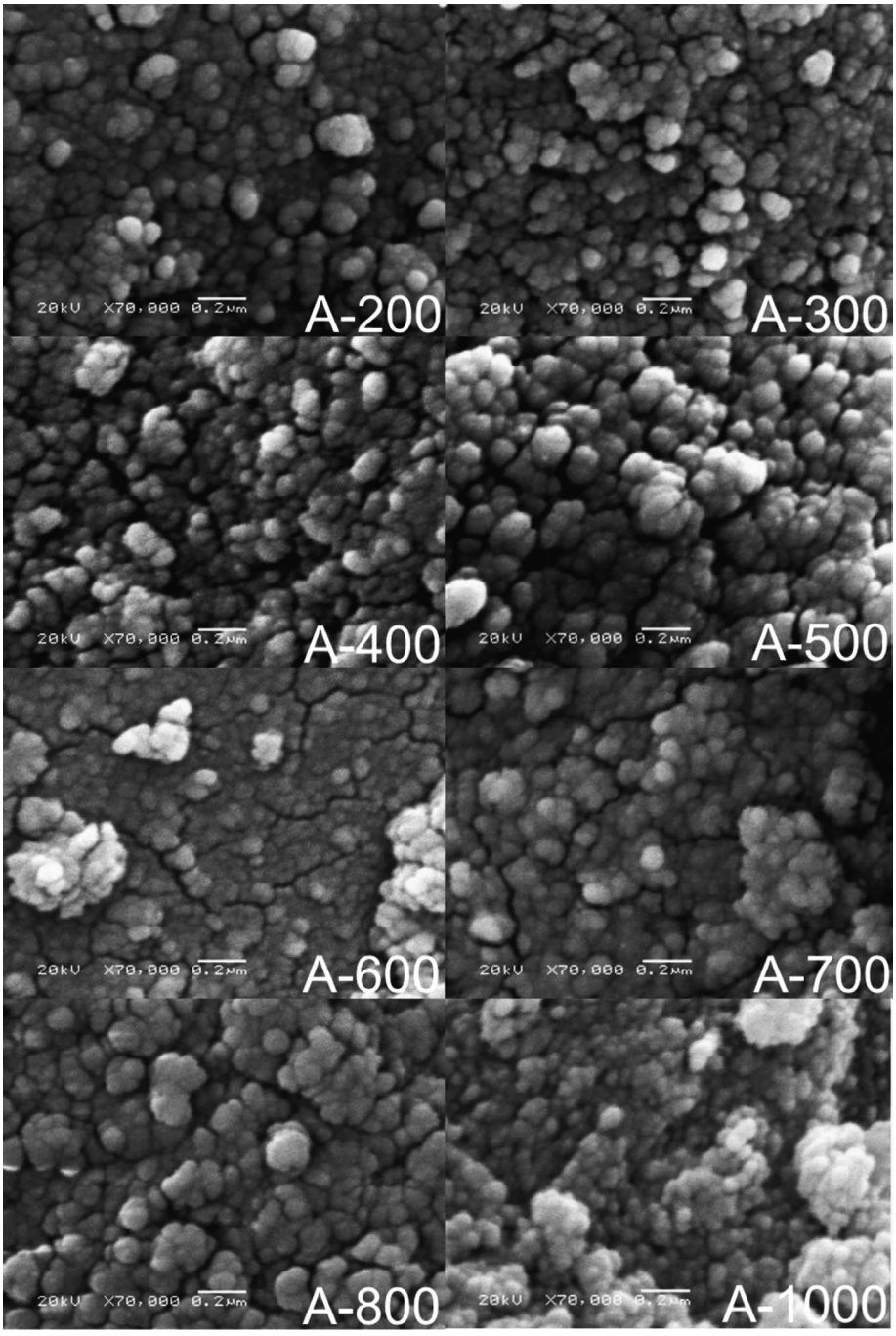

Fig. 5. Scanning electron micrographs of the calcined aluminas. The white bar is 200 nm, the magnification is 70,000.

desorption of water, although small amounts of residual organic matter may be entrapped in the aluminas even after calcination at higher temperatures. However, the carbon content is very low (ca. 0.2 wt%) and statistically the same for all aluminas. The number of the water molecules per nm^2 of the alumina surface can be calculated by

$$W(T\,^{\circ}\mathrm{C}) = \frac{\Delta m}{M_{\mathrm{H_2O}}} \cdot \frac{1}{A_{\mathrm{BET}} \cdot m_{\mathrm{i}}} \cdot N_{\mathrm{A}}, \tag{2}$$

where ($W(T\,^{\circ}\mathrm{C})$ is the number of water molecules per nm^2) of alumina surface at a given temperature, Δm is the weight loss at a given temperature (g), m_{i} is the initial weight of the alumina sample (g), $M_{\mathrm{H_2O}}$ is the molar mass of water (18.0153 g/mol), N_{A} is Avogadro's number ($6.022 \times 10^{23}\ \mathrm{mol}^{-1}$), and A_{BET} is the surface area determined by the BET method (nm^2/g). To evaluate the water adsorption capacity or hydrophilicity of the calcined aluminas, we also placed these calcined aluminas into a chamber with controlled humidity and temperature for 13 days (relative humidity, $88 \pm 3\%$ and $25 \pm 3\,^{\circ}\mathrm{C}$). After this period, the alumina were taken out and placed into airtight closed flasks while awaiting the TGA results. These hydrated aluminas evolved some amount of water while standing, in-

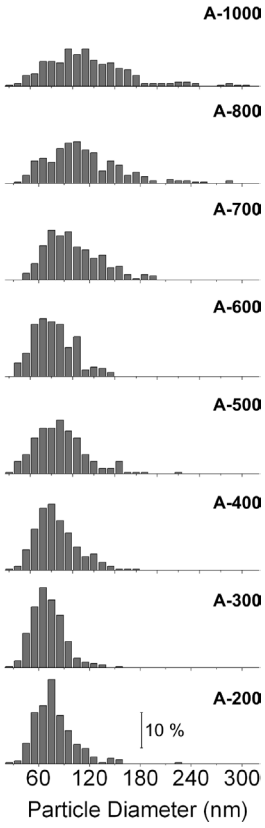

Fig. 6. Distribution of the particle diameters for calcined alumina ($n = 256$).

Table 3
Evolution of the average particle diameter ($n = 256$) for calcined aluminas A-200 to A-1000

Alumina	Average particle diameter (nm)	Standard deviation (nm)
A-200	79	24
A-300	71	20
A-400	81	25
A-500	86	30
A-600	77	24
A-700	100	32
A-800	113	44
A-1000	119	49

dicating that they were supersaturated with water. Thus, we dried the excess water condensed on the flask walls and performed the TGA once condensation was no longer observed (around two to three days). It is important to point out that after this procedure, no powder agglomerates were formed, and the samples appeared homogeneous. The values of $W(25\,^{\circ}\mathrm{C})$ for the original calcined (mildly rehydrated) samples, the values of $W_{\mathrm{hyd}}(25\,^{\circ}\mathrm{C})$ for controlled rehydrated samples, and the ratio $W_{\mathrm{hyd}}(25\,^{\circ}\mathrm{C}):W(25\,^{\circ}\mathrm{C})$ are given in Table 4.

The values obtained for the hydration of the γ-Al_2O_3 surfaces (A-400, A-500, and A-600), $W(25\,^{\circ}\mathrm{C})$, are of the same order of magnitude as those determined by De Boer et al. [36] for γ-Al_2O_3 after evacuation at 25 °C during 100 h or after drying at 120 °C (13 and 8.25 water molecules per nm^2, respectively). The most well-hydrated aluminas are A-200 and A-300

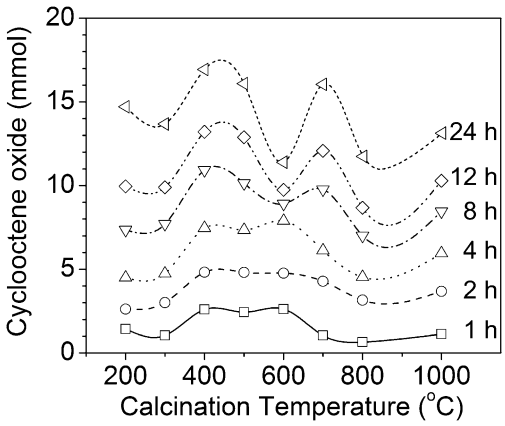

Fig. 7. Profiles of cyclooctene oxide yield for calcined aluminas at different reaction times. Reaction conditions: 20 mmol of *cis*-cyclooctene, 10 mmol of di-*n*-butylether, 56 mmol of H_2O_2 (70 wt%) and 200 mg of calcined alumina; $T = 80\,^{\circ}\mathrm{C}$.

Table 4
Number of water molecules per nm^2 for calcined aluminas, $W(25\,^{\circ}\mathrm{C})$, and aluminas hydrated in a humidity chamber, $W_{\mathrm{hyd}}(25\,^{\circ}\mathrm{C})$, and the ratio between these values

Alumina	$W(25\,^{\circ}\mathrm{C})$	$W_{\mathrm{hyd}}(25\,^{\circ}\mathrm{C})$	$\frac{W_{\mathrm{hyd}}(25\,^{\circ}\mathrm{C})}{W(25\,^{\circ}\mathrm{C})}$
A-200	20.2 ± 0.2	38.9 ± 1.4	1.93 ± 0.04
A-300	19.1 ± 0.2	39.6 ± 1.5	2.08 ± 0.08
A-400	11.6 ± 0.5	44.3 ± 2.9	3.58 ± 0.29
A-500	12.6 ± 0.2	40.6 ± 2.3	3.23 ± 0.05
A-600	12.5 ± 0.5	36.2 ± 0.4	2.89 ± 0.12
A-700	12.5 ± 0.1	31.7 ± 1.1	2.53 ± 0.09
A-800	12.7 ± 0.4	21.3 ± 0.4	1.68 ± 0.06
A-1000	11.8 ± 0.2	15.2 ± 0.2	1.29 ± 0.03

(ca. 20 water molecules per nm^2), which have the boehmite structure that contains water. None of the transition aluminas actually contains water in its structure [2,4], even though its surface can be highly hydroxylated. For A-400, which is mainly γ-Al_2O_3, the amount of water per nm^2 on the surface at 25 °C is quite small (i.e., ca. 11 water molecules per nm^2) compared with that for boehmites A-200 and A-300. Increasing calcination temperature progressively reduces the amount of water on the surface; however, the decrease in surface area makes the relative amount of water per nm^2 nearly constant (12 water molecules per nm^2). On the other hand, we observed that the exposure to controlled humidity (in a humidity chamber) caused extensive and quite different surface hydration, $W_{\mathrm{hyd}}(25\,^{\circ}\mathrm{C})$, of aluminas A-400 to A-1000. On the whole, it appears that hydrophilicity is declining in these aluminas.

In the catalytic epoxidation of *cis*-cyclooctene, the calcined aluminas showed different behaviors with respect to the yield of cyclooctene oxide (Fig. 7). This result was expected because calcination in the range of 200–1000 °C strongly changes the structural, textural, and chemical properties of the aluminas. It is possible to see two maxima at 400 and 700 °C at 24 h that correspond to 85 and 80% yields, respectively. This profile was already observed for the epoxidation of cyclohexene [22]. Interestingly, the catalytic activity was approximately the same for aluminas A-400, A-500, and A-600 at the beginning of the

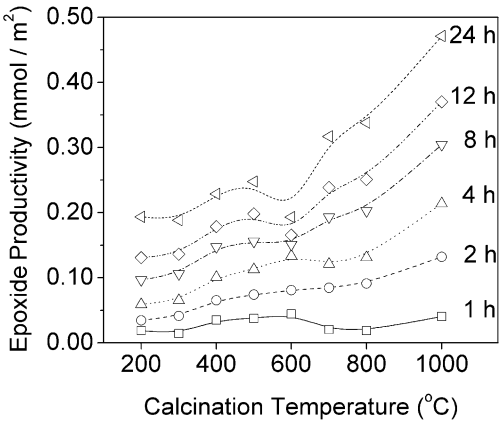

Fig. 8. Profiles of cyclooctene oxide productivity at different reaction times. Reaction conditions: 20 mmol of *cis*-cyclooctene, 10 mmol of di-*n*-butylether, 56 mmol of H_2O_2 (70 wt%) and 200 mg of calcined alumina; $T = 80\,^{\circ}C$.

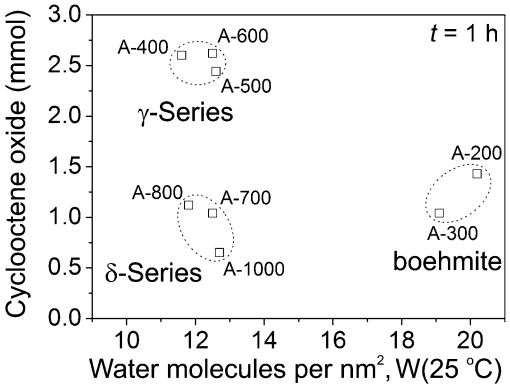

Fig. 9. Relation between the water molecules per nm^2 on the surface of aluminas and the epoxide yield at 1 h.

reactions (1 h). This trend held during the first 4 h. However, alumina A-600 deactivated at 4–8 h of reaction and gave only a 57% epoxide yield after 24 h. This fact is quite surprising, although it has been observed for other nanocrystalline aluminas synthesized and calcined at 600 °C [22]. The cause of the faster deactivation of the aluminas calcined at this temperature is not clear.

All aluminas calcined in the range of 200–1000 °C have catalytic activity for epoxidation using hydrogen peroxide, because the reaction without alumina produces yields of only ca. 15% after prolonged reaction time (12–24 h) [22,24]. Nonetheless, neither the behavior of the surface area nor the structural properties of the calcined aluminas can be directly related to the epoxide yields at different reaction times. Interestingly, analysis of the epoxide yield per unit of surface area (Fig. 8) demonstrates that epoxide productivity increases with increasing calcination temperature.

In a previous report [24], we observed that despite structural, textural, and acid–base properties, hydration of the γ-Al_2O_3 surface was the crucial factor in obtaining highly active aluminas for the epoxidation of olefins. Relating the values of $W(25\,^{\circ}C)$ with the epoxide yield after 1 h of reaction shows that the different aluminas are clustered in three distinct groups (Fig. 9), corresponding to the general classification of these aluminas' structure: boehmite; γ-series (including γ-Al_2O_3 and other forms); and δ-series (including δ-Al_2O_3, θ-Al_2O_3, and other forms). The differences between γ- and δ-series lie in the (i) crystallinity (the latter series shows better defined XRD pattern) and (ii) defect sites on the surface (the latter group has an extensively dehydrated surface with many defect sites, i.e., Lewis acid sites) [11,12]. Consequently, the surface hydrophilicity directly connects the structural properties of the calcined aluminas to their catalytic activity in the epoxidation of cyclooctene. Approximately the same correlation can be made when considering the epoxide productivity per unit of surface area at 1 h; however, alumina A-1000 is displaced from the δ-series to the γ-series cluster.

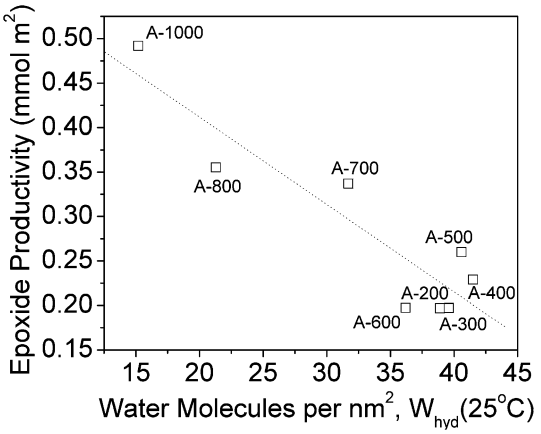

Fig. 10. Relation between the water molecules per nm^2 on the surface of aluminas (controlled hydrated), $W_{hyd}(25\,^{\circ}C)$, and epoxide productivity at 24 h.

Interestingly, the aluminas calcined in the range of 400–1000 °C show nearly the same initial surface hydration. However, at longer reaction times, they demonstrate significant differences in epoxide productivity. Analyzing the values $W_{hyd}(25\,^{\circ}C):W(25\,^{\circ}C)$, representing the water adsorption capacity or surface hydrophilicity, reveals large differences among these aluminas. The most hydrophilic alumina, A-400, has $W_{hyd}(25\,^{\circ}C):W(25\,^{\circ}C)$ around 3.6; in the least hydrophilic alumina, A-1000, this ratio is only 1.3. The boehmites appear as outliers in the correlation between water adsorption capacity and epoxide productivity at 24 h. The reason for this is that these aluminas already show a highly hydrated surface at the beginning of the reaction ($W(25\,^{\circ}C) \approx 20$ molecules of water per nm^2), and for a corrected comparison we must compare the absolute hydration of theses surfaces after water saturation, $W_{hyd}(25\,^{\circ}C)$, with the epoxide productivity at 24 h (Fig. 10). This correlation is in reasonable agreement with a linear model, $|r^2| = 0.92$, indicating that the approach of the olefin to the active sites is the limiting step at higher surface hydration.

Hydrogen peroxide is prone to decomposition into water and molecular oxygen in the presence of acids and bases [37]. It is known from the literature [11,12] that calcination of alumina at high temperatures produces vacancies that can act as strong Lewis acid sites (–O–Al^{3+}–O–). The rehydration of these sites gives Al–(O^+H_2) groups that, depending on the neighborhood of the aluminum ion, can act as moderate to strong Brønsted acid sites [8,11]. We believe that strong Brønsted acid sites

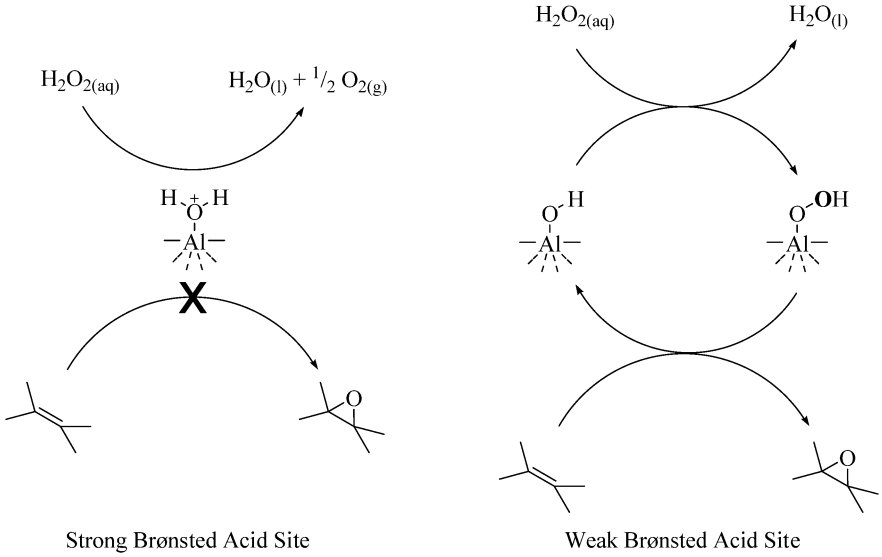

Fig. 11. Proposed role of the strong and weak Brønsted acid sites. The distal oxygen (in bold) from the Al–OOH species is believed to be transferred to the olefin.

present on the surface were responsible for the decomposition of hydrogen peroxide at the beginning of the reaction. More evidence for this was provided by the lower epoxide selectivity in the first 2 h of reaction (80–90%) compared with selectivity after prolonged reaction times (>95%). However, these ring-opening products or oligomers were not observed by GC analysis, indicating that these molecules are irreversibly adsorbed on the surface (as indicated by a considerable increasing of the carbon content on the alumina, ca. 5 wt%) and may poison the alumina surfaces. Work is in progress to clarify the changes occurring on the alumina surface during the reactions.

The weak to moderate Brønsted acid sites, Al–OH, behave more like hydroxy groups. Because of their high mobility, they can be easily replaced on the alumina surface by hydrogen peroxide, creating hydroperoxy groups on the surface that, due to the polarizing effect of the aluminum ions, can activate the O–O bond, facilitating distal oxygen transfer to the olefin (Fig. 11).

Interestingly, the aluminas from the γ-series (A-400, A-500, and A-600) and δ-series (A-700, A-800, and A-1000) had approximately the same amount of water on the surface per nm^2 (ca. 12 water molecules per nm^2). However, the epoxide yield after 1 h was much higher for the γ-series (ca. 12%) than for the δ-series (ca. 4%) (Fig. 9). This is because the γ-series aluminas have suitable strength in the acid sites at the beginning of the reaction, as a result of their weaker Al–OH groups than those of the δ-series aluminas [11]. Monitoring hydrogen peroxide consumption for all calcined aluminas revealed that the efficiency of the oxidant after the first hour of reaction was higher for aluminas from the γ-series (ca. 2.3 H_2O_2 per epoxide) than for those from the δ-series (ca. 4.1 H_2O_2 per epoxide). Boehmite, which is less acidic, showed somewhat better oxidant efficiency after 1 h of reaction (ca. 2.1 H_2O_2 per epoxide). Table 5 gives the oxidant efficiencies for all aluminas and reaction times.

For the δ-series aluminas, the consumption of hydrogen peroxide per epoxide formed (Table 5) was higher at initial reaction times, meaning that the surface was strongly modified at the beginning of the reactions (1–2 h). This reaction may consume the strong Brønsted acid sites and generate weaker Brønsted acid sites. After 2 h, the oxidant efficiency improved from ca. 4.1 to 2.3 hydrogen peroxide consumed per epoxide formed. For longer reaction times, the oxidant efficiency remained nearly constant for all calcined aluminas. Remarkably, alumina A-700 had better overall oxidant efficiency (ca. 1.9 H_2O_2 per epoxide) than A-400 (ca. 2.4 H_2O_2 per epoxide). Investigations are underway to rationalize these modifications of the surface during the reaction.

Table 5
Oxidant efficiency of the calcined aluminas at different reaction times

Alumina	Oxidant efficiency (mmol H_2O_2 per mmol of epoxide)					
	1 h	2 h	4 h	8 h	12 h	24 h
A-200	1.7	1.6	1.6	1.7	1.7	1.7
A-300	2.5	1.8	2.2	2.2	2.2	2.1
A-400	2.6	2.7	2.5	2.4	2.4	2.4
A-500	2.2	2.5	2.5	2.6	2.6	2.5
A-600	2.2	2.3	2.2	2.4	2.4	2.4
A-700	3.9	1.9	2.0	1.7	1.8	1.9
A-800	2.9	2.4	2.5	2.5	2.3	2.4
A-1000	5.5	2.6	2.5	2.4	2.3	2.5

4. Conclusion

Hydration of the alumina surface plays a pivotal role in the activities of the aluminas for catalytic epoxidation using the friendly oxidant aqueous hydrogen peroxide (70 wt%). In the beginning of the reaction (1 h), and considering the number of water molecules per nm^2, it is possible to segregate the aluminas obtained by calcination in the range of 200–1000 °C into three groups with different epoxidation activities. These groups correspond to the general classification of these aluminas' structures: boehmite, γ-series (including γ-Al_2O_3 and other forms), and δ-series (including δ-Al_2O_3, θ-Al_2O_3, and other forms). The difference between these alumina series is in

their crystallinity and the strength of their acid sites. This result is quite interesting, because until now it was not possible to show a relationship between structural, textural, and acidic properties and epoxide yields. High-temperature aluminas (i.e., aluminum oxides from the δ-series) have high catalyst activity at the beginning of the reaction. We believe that the strong Brønsted acid sites decompose the hydrogen peroxide during the first hour of reaction. Important (although yet unknown) changes in the alumina surface occurring during the first hour of the reaction improve oxidant efficiency from 3.9 mmol of hydrogen peroxide consumed per mmol of epoxide formed after 1 h to 1.9 mmol of hydrogen peroxide consumed per mmol of epoxide formed after 24 h for alumina calcined at 700 °C. The best yields for cyclooctene oxide were 85% obtained with the aluminas calcined at 400 °C and 80% obtained with those calcined at 700 °C. However, in terms of oxidant efficiency, the alumina calcined at 700 °C (A-700) is better, because it consumes less hydrogen peroxide (1.9 H_2O_2 per epoxide formed) than A-400 (2.4 H_2O_2 per epoxide formed). The selectivity for epoxide was always >95%, indicating that the strong acid sites do not survive for long under these reaction conditions. If the strong acid sites were still present during the reactions, then the selectivity for epoxide would be lower due to acid-catalyzed ring opening, forming diols and oligomers.

The water adsorption capacity or hydrophilicity of these aluminas shows a strong correlation with the epoxide productivity of the calcined aluminas. Aluminas calcined at higher temperatures have better epoxide productivity per unit of surface area because of their lower hydrophilicity. Therefore, there is an interesting paradox for alumina-catalyzed olefin epoxidation: The catalytically active sites, weak to moderate Brønsted acid sites (Al–OH), can act as an inhibitor of the catalytic cycle if the surface is too highly hydroxylated, because the hydrophobic olefins cannot approach the alumina surface for oxygen transfer from the Al–OOH groups; however, the weak to moderate Brønsted acid sites (Al–OH), found mainly on highly hydroxylated alumina surfaces, are necessary for the activation of hydrogen peroxide. We are working to develop methods of improving the hydrophobicity of the alumina surface without killing these active sites, which is proving not a trivial task.

Acknowledgments

The authors are grateful to FAPESP and CNPq for financial support and to Peróxidos do Brasil (Solvay) for the supply of 70 wt% aqueous hydrogen peroxide (Interox 70-10). R.R. is also grateful to Leandro Gomes Moreira for helping with some parts of the experimental work. The authors thank Carol Collins for her careful reading of the manuscript.

References

[1] L.K. Hudson, C. Misra, A.J. Perrotta, K. Wefers, F.S. Williams, Ullmann's Encyclopedia of Industrial Chemistry, Electronic Release, seventh ed., VCH, Weinheim, 2004.
[2] C. Misra, Industrial Alumina Chemicals, American Chemical Society, Washington, 1986.
[3] M. Breysse, P. Afanasiev, C. Geantet, M. Vrinat, Catal. Today 86 (2003) 1.
[4] G.W. Kabalka, R.M. Pagni, Tetrahedron 53 (1997) 7999.
[5] J. Sanchez-Valente, X. Bokhimi, J.A. Toledo, Appl. Catal. A 264 (2004) 175.
[6] T. Tsukada, H. Segawa, A. Yasumori, K. Okada, J. Mater. Chem. 9 (1999) 549.
[7] J.J. Fitzgerald, G. Piedra, S.F. Dec, M. Seger, G.E. Marciel, J. Am. Chem. Soc. 119 (1997) 7832.
[8] H. Knözinger, P. Ratnasamy, Catal. Rev.-Sci. Eng. 17 (1978) 31.
[9] P. Tundo, Continuous Flow Methods in Organic Synthesis, Ellis Horwood, New York, 1991.
[10] J.B. Peri, J. Phys. Chem. 69 (1965) 211.
[11] K. Tanabe, Solid Acids and Bases and Their Catalytic Properties, Academic Press, New York, 1970.
[12] K. Tanabe, M. Misono, Y. Ono, H. Hattori, New Solid Acids and Bases and Their Catalytic Properties, Elsevier, Amsterdam, 1989.
[13] B. Kasprzyk-Hordern, Adv. Colloid Interface Sci. 110 (2004) 19.
[14] G.W. Kabalka, R.M. Pagni, Tetrahedron 53 (1997) 7999.
[15] G.H. Posner, Angew. Chem. Int. Ed. Engl. 17 (1978) 487.
[16] D. Mandelli, M.C.A. van Vliet, U. Arnold, R.A. Sheldon, U. Schuchardt, J. Mol. Catal. A: Chem. 168 (2001) 165.
[17] J. Rebek, R. McCready, Tetrahedron Lett. (1979) 4337.
[18] D. Mandelli, M.C.A. van Vliet, R.A. Sheldon, U. Schuchardt, Appl. Catal. A: Gen. 219 (2001) 209.
[19] M.C.A. van Vliet, D. Mandelli, I.W.C.E. Arends, U. Schuchardt, R.A. Sheldon, Green Chem. 3 (2001) 243.
[20] R.G. Cesquini, J.M.S. Silva, C.B. Woitiski, D. Mandelli, R. Rinaldi, U. Schuchardt, Adv. Synth. Catal. 344 (2002) 911.
[21] I.W.C.E. Arends, R.A. Sheldon, Topics Catal. 19 (2002) 133.
[22] R. Rinaldi, J. Sepulveda, U. Schuchardt, Adv. Synth. Catal. 346 (2004) 281.
[23] J.E. Leffer, D.W. Miller, J. Am. Chem. Soc. 99 (1977) 480.
[24] R. Rinaldi, U. Schuchardt, J. Catal. 227 (2004) 109.
[25] W.A. Herrmann, R.W. Fischer, D.W. Marz, Angew. Chem. Int. Ed. Engl. 30 (1991) 1638.
[26] J.A. Wang, X. Bokhimi, A. Morales, O. Novaro, T. López, R. Gómez, J. Phys. Chem. B 103 (1999) 299.
[27] F. Vaudry, S. Khodabandeh, M. Davis, Chem. Mater. 8 (1996) 1451.
[28] H.L. Fleming, K.P. Goodboy, in: L.D. Hart (Ed.), Alumina Chemicals: Science and Technology Handbook, The American Ceramic Society, Washington, 1990, p. 251.
[29] H. Kraus, M. Müller, R. Prins, A.P.M. Kentgens, J. Phys. Chem. B 102 (1998) 3862.
[30] C. Wolverton, K.C. Hass, Phys. Rev. B 63 (2000) 024102.
[31] B.C. Lippens, J.H.D. Boer, Acta Crystallogr. 17 (1964) 1312.
[32] R. Zhou, R.L. Snyder, Acta Crystallogr. B 47 (1991) 617.
[33] G.K. Priya, P. Padmaja, K.G.K. Warrier, A.D. Damodaran, G. Aruldhas, J. Mater. Sci. Lett. 16 (1997) 1584.
[34] K.A. Wickersheim, G.K. Korpi, J. Chem. Phys. 42 (1965) 579.
[35] S.J. Gregg, K.S.W. Sing, Adsorption, Surface Area and Porosity, Academic Press, New York, 1982.
[36] J.H. De Boer, J.M.H. Fortuin, B.C. Lippens, W.H. Meijs, J. Catal. 2 (1965) 1.
[37] F.A. Cotton, G. Wilkinson, C.A. Murillo, M. Bochmann, Advanced Inorganic Chemistry, sixth ed., Wiley–Interscience, New York, 1999, p. 458.